A SEMI-SUPERVISED METHOD FOR NONLINEAR HYPERSPECTRAL UNMIXING

Bikram Koirala, Paul Scheunders

Imec-Visionlab, University of Antwerp, Belgium

ABSTRACT

As the interaction of light with the Earth surface is very complex, spectral reflectances are composed of nonlinear mixtures of the observed materials. Nonlinear mixing models have the disadvantage that not all spectra of a hyperspectral dataset necessarily follow the same particular mixing model. Moreover, most models lack a proper interpretation of the estimated parameters in terms of fractional abundances. In this paper, we present a semi-supervised nonlinear unmixing technique that overcomes these problems. In a first step, we apply a kernelized simplex volume maximization to select an overcomplete set of endmembers that precisely describe the hyperspectral data manifold. In a second step, this set is used as ground truth data in a supervised learning approach to generate fractional abundance maps from the entire dataset. For this, three methods are presented, based on kernelized sparse unmixing, feedforward neural networks, and gaussian processes. The proposed method is validated on simulated data, a dataset obtained by ray tracing, and a real hyperspectral image.

1. INTRODUCTION

To estimate the fractional abundances of the different materials within a hyperspectral pixel, the error between the pixels true reflectance spectrum and the spectrum that is generated by a particular mixing model is minimized. Traditionally, the linear mixing model (LMM) is assumed, which is valid when the incoming rays of light interact with a single pure material in the pixels instantaneous field of view (IFOV) before reaching the sensor. The reconstruction error can be minimized using the Fully Constrained Least Squares Unmixing procedure (FCLSU) [1], that takes the physical non-negativity and sum to one constraints of the fractional abundances into account.

To model multiple interactions of the light with more than one pure material, nonlinear mixing models have been developed. Some examples are the bilinear mixing models that describe the interaction of an incident ray of light with two pure materials [2], extensions of these, e.g. the multilinear mixing model (MLM) [3], and intimate mixture models such as the Hapke model [2].

One of the unsolved problems is that not all spectra of a hyperspectral dataset may follow the same particular mixing model. Another problem is that most nonlinear mixing models are unable to properly interpret and link the estimated model parameters to the actual fractional abundances. Recently, we proposed a model-independent supervised nonlinear unmixing method [4], that learns a mapping between the actual nonlinear spectra and linearly mixed spectra, after which FCLSU can be applied to obtain the actual fractional abundances. The disadvantage of this method is that it requires a large number of ground truth mixed pixels. In this work, we propose a semi-supervised approach, hereby limiting the required number of training data.

The first step in the approach is the use of SAGA [5], a method that uses kernelized simplex volume maximization (KSVM) to pick an overcomplete set of endmembers from the hyperspectral dataset that characterizes the manifold hull. Among the selected endmembers, some may be spectra of pure materials but most of them are in itself mixture of pure materials. In a second step, the overcomplete set of endmembers and their actual fractional abundances are used as ground truth training data in a supervised learning approach to generate fractional abundance maps of the entire dataset. For this, three methods are presented, based on kernelized sparse unmixing, feedforward neural networks, as in [4], and gaussian processes.

2. METHODOLOGY

In [5], SAGA, a kernelized extension of Nonnegative Matrix Factorization (NMF) is presented. NMF decomposes a given matrix of spectra $\mathbf{X} = [\mathbf{x}_1, \cdots, \mathbf{x}_n]$ into a product of an endmember matrix $\mathbf{F}$ ($\{\mathbf{f}_i\}_{i=1}^{l} \in \mathbf{R}_+^d$) and a matrix of abundances $\mathbf{G}$ ($\{\mathbf{g}_i\}_{i=1}^{n} \in \mathbf{R}_+^l$). $\|\mathbf{X} - \mathbf{FG}\|^2$ is minimized under the nonnegativity and sum to one constraints.

SAGA performs the matrix factorization, after projecting the original dataset onto an infinite dimensional feature space ($\mathbf{X} \rightarrow \phi(\mathbf{X})$). $\|\phi(\mathbf{X}) - \phi(\mathbf{F})\mathbf{G}\|^2$ is then minimized.

SAGA performs the matrix factorization in two steps. In the first step, kernelized simplex volume maximization (KSVM) is used to generate an overcomplete set of endmembers $\mathbf{F}$. The selected points are supposed to precisely characterize the data manifold (see Fig. 1). To characterize a nonlinear data manifold, a large number of data points is required. But the intrinsic dimensionality of the dataset can be very low. Among the overcomplete set of selected endmembers, few will be pure materials while most are in itself

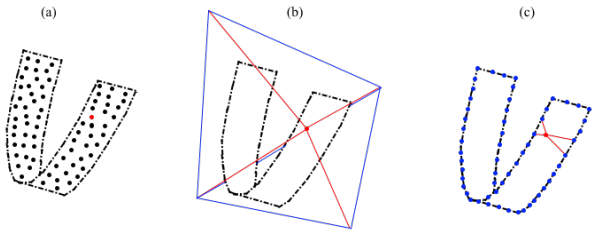

Fig. 1: (a) A dataset $\mathbf{X}$ sampled from a U-shaped manifold; (b) a convex hull (simplex) embeds the dataset and describes each data point by barycentric coordinates; (c) selection of an overcomplete set of points to characterize the manifold hull.

mixtures of pure materials.

In the second step, the matrix $\mathbf{G}$ is determined by Kernelized Fully Constrained Sparse Unmixing (KFCSU). This amounts to solving n independent problems of estimating the columns of $\mathbf{G}$:

$$\mathbf{g}_i = arg\min_{\mathbf{g}_i} \|\boldsymbol{\phi}(\mathbf{x}_i) - \boldsymbol{\phi}(\mathbf{F})\mathbf{g}_i\|^2 \quad (1)$$

s.t. $\sum_{j=1}^{l} g_{ji} = 1, g_{ji} \geq 0, \forall j$. To enforce sparsity ($\lambda < l$), the previous constraints are replaced by $\sum_{j=1}^{\lambda} g_{ji} = 1, \sum_{j=\lambda+1}^{l} g_{ji} = 0, g_{ji} \geq 0, \forall j$. As a result, the fractional abundances of the hyperspectral pixels in terms of the overcomplete set of endmembers are obtained:

$$\boldsymbol{\phi}(\mathbf{x}_i) = g_{1i}\boldsymbol{\phi}(\mathbf{f_1}) + \cdots + g_{\lambda i}\boldsymbol{\phi}(\mathbf{f}_\lambda) + 0\boldsymbol{\phi}(\mathbf{f}_{\lambda+1}) + \cdots + 0\boldsymbol{\phi}(\mathbf{f}_l) \quad (2)$$

To estimate the true fractional abundances of a hyperspectral pixel, we propose to use a supervised approach in which we assume that the actual fractional abundances of the selected endmember set are known as ground truth. We then assume that the actual abundances of a pixel will be composed of the ground truth abundances by the same linear combination as in (2):

$$\mathbf{a}_i = g_{1i}\mathbf{a}_{\mathbf{f_1}} + \cdots + g_{\lambda i}\mathbf{a}_{\mathbf{f}_\lambda} + 0\mathbf{a}_{\mathbf{f}_{\lambda+1}} + \cdots + 0\mathbf{a}_{\mathbf{f}_l} \quad (3)$$

where $\mathbf{a}_{\mathbf{f}_j}$ is the ground truth fractional abundance of endmember $\mathbf{f}_j$ and $\mathbf{a}_i$ is the estimated true fractional abundance of the data point $\mathbf{x}_i$.

As an alternative strategy to obtain the fractional abundances, the ground truth abundances are applied to generate linearly mixed spectra of the overcomplete endmember set. After that, the mapping of their true reflectance spectra to these linearly mixed spectra is learned. When applying the learned map to the pixels spectra $\mathbf{X}$, linear spectral $\mathbf{X}_l$ are obtained. Finally, these mapped spectra are unmixed by using FCLSU to estimate the fractional abundances.

The learning of this mapping can be performed in different ways. One way is the use of a feedforward neural network (NN), as in [4].

Another way to learn the nonlinear relationship between the input ($\mathbf{X}$) and output ($\mathbf{X}_l$) is given by gaussian processes (GP) [6]. GP is a bayesian method, in which the distribution of an infinite number of gaussian shaped basis functions is chosen as prior. Determining the posterior distribution is similar to specifying a gaussian kernel function:

$$k(\mathbf{x}_i, \mathbf{x}_j) = \sigma_f^2 \exp\left(-\sum_{b=1}^{d} \frac{\left(x_i^b - x_j^b\right)^2}{2l_b^2}\right) \quad (4)$$

where σ_f^2 is a scaling factor, and l_b is a characteristic length-scale for each band. The mean prediction for each data point according to GP is given by [6]:

$$\overline{\mathbf{x}}_l = f(\mathbf{x}) = \mathbf{X}_l[K(\mathbf{X}, \mathbf{X}) + \sigma_n^2\mathbf{I}]^{-1}\mathbf{k}_* \quad (5)$$

where $\mathbf{k}_* = k(\mathbf{x}, \mathbf{x}_*)$ is the vector of kernel functions between a test sample and the n training points and $K(\mathbf{X}, \mathbf{X})$ is the matrix of kernel functions between the n training points. σ_n^2 is the image noise variance. These model parameters are optimized by maximizing the marginal likelihood in the training dataset.

After the mapping of the nonlinear spectra to the linear model is learned, either by NN or GP, the mapped spectra are unmixed by FCLSU to estimate the fractional abundances.

3. EXPERIMENTAL RESULTS AND DISCUSSION

In this section, we validate the three proposed methods, i.e. the use of KSVM along with KFCSU, NN, and GP respectively.

3.1. Simulated data

In a first experiment, we generated 30000 nonlinear data points by using the Hapke model ([2]) and by randomly choosing three pure spectra from the USGS dataset. These spectra contain 224 bands with wavelengths in the range 383-2501 nm. The fractional abundances to mix these spectra were generated uniformly and randomly from the unit simplex.

The KSVM technique was used to select a limited number of points from the nonlinear data manifold, unmixing was performed using KFCSU, and Equation (3) was applied to generate the fractional abundances. Similarly, the fractional abundances of points selected by KSVM are applied to learn a mapping to the linear model by using either NN or GP, after which FCLSU was applied for an estimation of the abundance maps.

Figure 2 plots the average and standard deviation of the root mean squared error (RMSE) between the estimated and the true fractional abundance values for 100 runs (different sets of pure spectra and fractional abundances) as a function of the applied number of training samples. For this dataset,

GP clearly outperforms the other two methods, and low errors are obtained while a very limited amount of training samples is required.

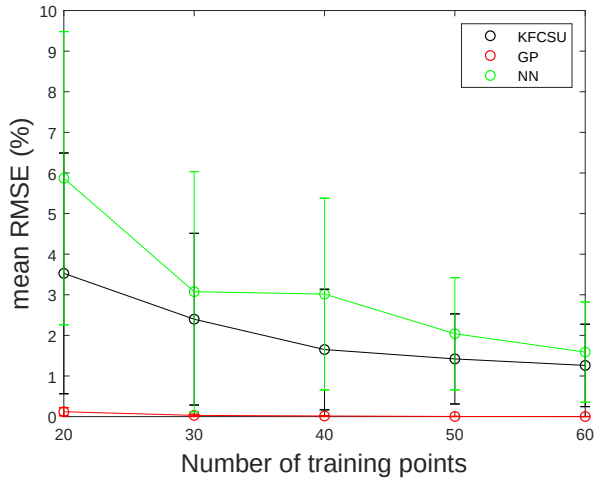

Fig. 2: RMSE (100 runs) obtained by the three proposed methods in function of the applied number of training samples.

3.2. Samson data

In the second experiment, the Samson dataset [7] was used, which can be downloaded from [1]. In this dataset, fractional abundances of three pure materials (soil, tree, water) for 9025 (95×95) pixels are available.

We selected 40 pixels using KSVM and used these for training, while the remaining 8985 pixels were used for testing the methods. Figure 3 displays the ground truth abundance maps, the abundance maps estimated by KFCSU, GP, and NN respectively, and the absolute differences between the ground truth and estimated abundance maps (rescaled to the maximal difference that was obtained over all three methods). For this dataset, KFCSU outperformed the other two methods. The obtained abundance RMSEs (%) for this dataset were 5.79, 7.68, and 9.20 for KFCSU, GP, and NN respectively. For comparison, when selecting the 40 training points randomly (100 runs) instead of using KSVM, the obtained RMSEs were 6.89 ± 1.00, 8.93 ± 1.12, and 11.43 ± 2.57 for KFCSU, GP, and NN respectively.

3.3. Ray tracing data

The third experiment was performed by using a dataset generated by ray tracing. It represents an orchard with mixtures of three endmembers: soil, weed patches, and citrus trees, [8]. This dataset contains ground truth fractional abundances for

[1] http://www.escience.cn/people/feiyunZHU/Dataset_GT.html

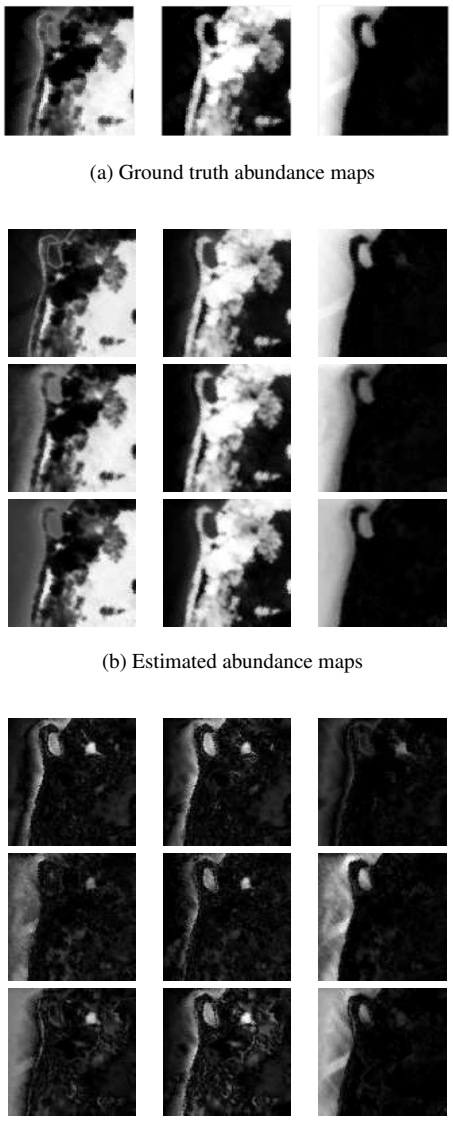

(a) Ground truth abundance maps

(b) Estimated abundance maps

(c) Absolute differences

Fig. 3: Samson dataset. (a) Ground truth abundance maps for soil, tree, and water respectively; (b) estimated abundance maps, from top to bottom, by KFCSU, GP, and NN respectively; (c) absolute differences between estimated and ground truth abundance maps, from top to bottom, by KFCSU, GP, and NN respectively.

400 (20×20) pixels. We selected 10 pixels by KSVM and used these for training while the remaining 390 pixels were applied for testing the methods.

Figure 4 displays the ground truth abundance maps, abundance maps estimated by the three methods, and the absolute differences between the ground truth and estimated abundance maps. For this dataset, GP outperformed the other two methods. The abundance RMSEs (%) for this dataset are 5.73, 2.06, and 3.46 for KFCSU, GP, and NN respec-

tively. For comparison, when selecting the 10 training samples randomly (100 runs) instead of using KSVM, the obtained RMSEs were 8.87±2.21, 4.33±2.43, and 11.19±4.71 for KFCSU, GP, and NN respectively.

(a) Ground truth abundance maps

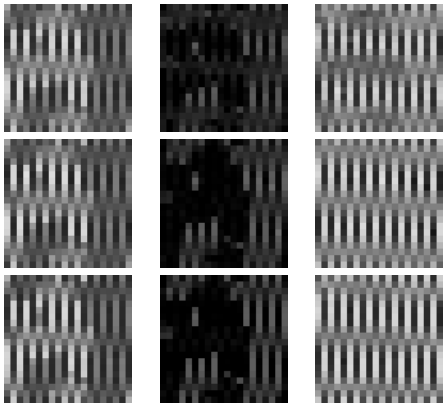

(b) Estimated abundance maps

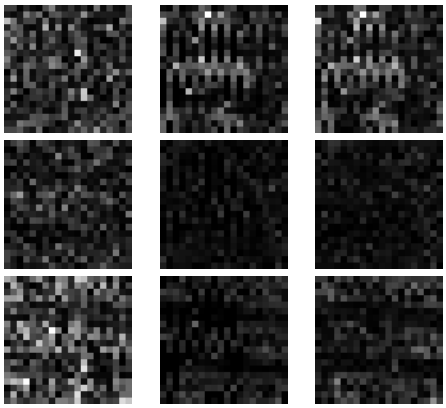

(c) Absolute differences

Fig. 4: Ray tracing data set. (a) Ground truth abundance maps for soil, weed, and tree respectively; (b) estimated abundance maps, from top to bottom, by KFCSU, GP, and NN respectively; (c) absolute differences between estimated and ground truth abundance maps, from top to bottom, by KFCSU, GP, and NN respectively.

4. CONCLUSIONS

In this paper, we proposed a model-independent semisupervised method for nonlinear spectral unmixing of hyperspectral data. The method is a combination of a simplex volume maximization step to extract an overcomplete endmember set that precisely describes the nonlinear manifold and three supervised approaches to estimate the fractional abundances. Experiments on simulated data, a ray tracing dataset and a true hyperspectral image show that this method is very promising. In future work, we will apply this method to parameter estimation of physical reflectance models.

Acknowledgement

The research presented in this paper is funded by BELSPO (Belgian Science Policy Office) in the frame of the STEREO III programme – project GEOMIX (SR/06/357).

5. REFERENCES

[1] J. W. Boardman, "Geometric mixture analysis of imaging spectrometry data," in *IEEE Intern. Geosci Remote Sens. Symp.*, 1994, pp. 2369–2371.

[2] R. Heylen, M. Parente, and P. Gader, "A review of nonlinear hyperspectral unmixing methods," *IEEE J. Sel. Topics Appl. Earth Observ. Remote Sens.*, vol. 7, no. 6, pp. 1844–1868, 2014.

[3] R. Heylen and P. Scheunders, "A multilinear mixing model for nonlinear spectral unmixing," *IEEE Trans. Geosci. Remote Sens.*, vol. 54, no. 1, pp. 240–251, 2016.

[4] B. Koirala, R. Heylen, and P. Scheunders, "A neural network method for nonlinear hyperspectral unmixing," in *IEEE Intern. Geosci Remote Sens. Symp.*, 2018, pp. 4233–4236.

[5] Nicolas Courty, Xing Gong, Jimmy Vandel, and Thomas Burger, "Saga: sparse and geometry-aware non-negative matrix factorization through non-linear local embedding," *Machine Learning*, vol. 97, no. 1, pp. 205–226, 2014.

[6] C.K.I. Williams C.E. Rasmussen, *Gaussian Processes for Machine Learning*, The MIT Press, New York, 2006.

[7] Feiyun Zhu, Ying Wang, Bin Fan, Shiming Xiang, Geofeng Meng, and Chunhong Pan, "Spectral unmixing via data-guided sparsity," *IEEE Trans. Image Process.*, vol. 23, no. 12, pp. 5412–5427, 2014.

[8] B. Somers, L. Tits, and P. Coppin, "Quantifying nonlinear spectral mixing in vegetated areas: Computer simulation model validation and first results," *IEEE J. Sel. Topics Appl. Earth Observ. Remote Sens.*, vol. 7, no. 6, pp. 1956–1965, 2014.